Rock and Soil Mechanics

Volume 42 | Issue 4 Article 7

8-25-2021

Effect of different notch prefabrication methods and notch lengths on rock three-point bending test

Hao LU
University of Chinese Academy of Sciences, Beijing 100049, China

Xia-ting FENG
Key Laboratory of Ministry of Education on Safe Mining of Deep Metal Mines, Northeastern University, Shenyang, Liaoning 110819, China

Cheng-xiang YANG
Key Laboratory of Ministry of Education on Safe Mining of Deep Metal Mines, Northeastern University, Shenyang, Liaoning 110819, China

Xi-wei ZHANG
Key Laboratory of Ministry of Education on Safe Mining of Deep Metal Mines, Northeastern University, Shenyang, Liaoning 110819, China, luhaosc@foxmail.com

Rock and Soil Mechanics 2021 42(4): 1115−1125 ISSN 1000−7598
https: //doi.org/10.16285/j.rsm.2020.6336 rocksoilmech.researchcommons.org/journal

Effect of different notch prefabrication methods and notch lengths on rock three-point bending test

LU Hao[1, 2], FENG Xia-ting[1, 3], YANG Cheng-xiang[3], ZHANG Xi-wei[3]

1. State Key Laboratory of Geomechanics and Geotechnical Engineering, Institute of Rock and Soil Mechanics, Chinese Academy of Sciences, Wuhan, Hubei 430071, China

2. University of Chinese Academy of Sciences, Beijing 100049, China

3. Key Laboratory of Ministry of Education on Safe Mining of Deep Metal Mines, Northeastern University, Shenyang, Liaoning 110819, China

Abstract: To select an appropriate notch prefabrication method and notch length for obtaining relatively accurate and reliable rock mode I fracture toughness (K_{IC}), as well as to improve understanding of macro fracture process and meso-fracture characteristics in the rock three-point bending test, three methods, i.e., wire cutting, saw blade cutting and water jet cutting were used to prefabricate notch in granite and marble specimens for three-point bending test. The comparison of micro fracture characteristics among three different cutting methods was conducted with the application of scanning electronic microscopic. The test results show that the effect of wire cutting method on K_{IC} is the smallest. In addition, three-point bending tests on granite and marble containing dimensionless notch length of 0.1, 0.2, 0.3, 0.4, and 0.5 show that K_{IC} tends to increase firstly and then decrease with increasing notch length. The dimensionless notch length of α=0.3 is recommended for obtaining the representative K_{IC}. The macroscopic failure of rock specimen undergoes a process of initiation of localization zone, development of localization zone, crack initiation, and finally fracture propagation. The acoustic emission process of rock specimen is observed with an obvious brittle characteristic, the crack opening displacement curve is consistent with the trend of cumulative acoustic emission curve, and the evolution of crack opening displacement curve can be regarded as a macroscopic characterization of the specimen internal failure development process.

Keywords: rock three-point bending test; mode I fracture toughness; notch prefabrication method; notch length; fracture process

1 Introduction

In 1921, Griffith's[1] research on low-stress brittle fracture of glass provided an experimental basis for the establishment of fracture mechanics. In 1948, Irwin[2] applied Griffith's fracture theory to the problem of metallic materials ductile-brittle fracture, which contributed to the establishment of fracture mechanics[3]. Irwin proposed the concept of stress intensity factor in 1957, and obtained the material stress intensity factor criterion[4] accordingly. Fracture toughness, that is, critical stress intensity factor, has become an important concept of linear elastic fracture mechanics.

The American Society for Testing and Materials (ASTM) has propelled the establishment of fracture toughness test standards. It has promulgated the first fracture toughness test standard for metals, ASTM E399-70T[5], which includes fracture toughness test methods of the compact tensile method and three-point bending method. China started research on fracture mechanics in 1968. A group of scientists including Chi Chen contributed in fracture mechanics test standards and stress intensity factor calibration, and they have been successfully applied in engineering fields such as aviation and nuclear power materials, which greatly boosted China's development in the field of fracture mechanics.

In the 1960 s, fracture mechanics theory was applied to geoscience research. Atkinson et al.[6] wrote the first rock fracture mechanics work in 1987, which expanded a new direction for rock mechanics, and rock fracture mechanics has gradually developed into an important branch of rock mechanics. The concepts in fracture mechanics are beneficial in describing the rock fracture process and explaining the fracture mechanism. As an important parameter in rock fracture mechanics, rock fracture toughness characterizes the ability of rock to resist new crack propagation. This index is used to analyze rock mechanics and engineering problems such as rock damage, blasting, and hydraulic fracturing[7−8]. Cracks are divided into mode I (opening tensile mode), mode II (in-plane shear mode) and mode III (out-of-plane shear mode). The initiation and propagation of tensile cracks in rock failure are the dominant factors in rock fracture. Therefore it is very important to test and study the mode I fracture toughness K_{IC}.

In order to test the rock K_{IC}, the International Society for Rock Mechanics (ISRM) and ASTM have issued

Received: 4 September 2020 Revised: 2 November 2020
This work was supported by the National Key Research and Development Program of China (2018YFC0407006).
First author: LU Hao, male, born in 1996, Master candidate, research interest: rock three-point bending experiment. E-mail: luhaosc@foxmail.com
Corresponding author: ZHANG Xi-wei, male, born in 1976, PhD, Professor, research interest: rock mechanics experiments. zhangxiwei@mail.neu.edu.cn

relevant recommended methods or standards. Some scholars have also proposed new test methods for rock K_{IC}. The statistical K_{IC} test methods are shown in Table 1, but so far, a unified test standard has not yet been formed. There are two main reasons why it is difficult to accurately test the fracture toughness of rock: 1. It is difficult to prefabricate notches of a specific shape and size and the length of the crack is difficult to accurately determine. 2. The test results of fracture toughness are affected by many influencing factors.

Table 1 Common test methods for rock K_{IC}

Test method	Abbreviation	Prefabricated notch	Literature
Single-Edge Notched Bending	SENB	Straight	ASTM[20]
Short Rod	SR	V-shaped	ISRM[8]
Chevron Bend	CB	V-shaped	ISRM[8]
Cracked Chevron Notched Brazilian Disk	CCNBD	Chevron	Fowell [21]
Semi-circular Bend	SCB	Straight	Kuruppu et al.[22]
Cracked Chevron Notched Semi-circular Bending	CCNSCB	Chevron	Kuruppu[23]
Straight Notched Disk Bending	SNDB	Straight	Tutluoglu et al.[24]
Edge cracked triangular	ECT	Straight	Aliha et al.[25]

Many scholars have carried out research on the influence of factors including the geometric size and shape of the sample[9], temperature[10], confining pressure[11], mesoscopic parameters[12], rock and mineral particle size [13], and test methods[14] on rock K_{IC} test results, but the basic notch prefabrication method is not consistent. Zhao et al.[15] studied the influence of bedding on the K_{IC} of shale using the prefabricated Semi-circular Bend specimen by the wire cutting method. Cui et al.[16] used the saw blade cutting method to determine the K_{IC} of sandstone on the prefabricated cracked chevron notched Brazilian disk samples. In the research on rock three-point bending test, three prefabrication methods are mainly used to prefabricate artificial notches in rock specimens: wire cutting, saw blade cutting and waterjet cutting. However, the influence of different notch prefabrication methods has not been compared and studied. The influencing factors of notch prefabrication method have not been paid enough attention. Huang et al.[17] pointed out that the influence of rock notch prefabrication method on fracture toughness needs further study to find a set of test methods suitable for rock characteristics. Zheng et al. [18] conducted K_{IC} test comparisons on either prefabricated fatigue cracks or narrow notches of single-edge notched bending specimens of four types of rocks and found that the K_{IC} of fatigue cracked specimens was greater than the test results of narrow notch specimens. Combining the difficulty of prefabrication and actual conditions, it is recommended to use narrow-notch specimens for rock K_{IC} testing of application considerations. Tian et al.[19] compared the K_{IC} value of concrete with pre-inserted notch and sawed notch and found that the former is smaller than the latter. The notch prefabrication method has an impact on the K_{IC} test results, but the effect of the commonly used notch prefabrication method on the rock K_{IC} test results is still unclear.

Regarding the influence of prefabricated notch length on rock fracture toughness, Zhang et al.[26] studied the influence of notch length on K_{IC} using a straight notched semi-circular bend specimen, and found that within the dimensionless notch length range of 0.3 to 0.7, the K_{IC} value gradually decreases as the notch length increases. Wang et al.[27] prefabricated granite specimens with different notch lengths and measured the pattern that the peak fracture load gradually decreases with the increase of the notch length. Sun et al.[28] gave the rule that the K_{IC} test values of short rod samples first increase and then decrease with increasing the notch length. Different prefabricated notch lengths for K_{IC} testing will cause differences in results. For single-edge notched bending specimens (SENB), ASTM recommends prefabricating notch with a dimensionless length of 0.5[20]. Since this method is proposed for metals, it was also widely used in rock K_{IC} testing subsequently, but the prefabricated notch length that can obtain a relatively accurate rock K_{IC} value has not yet been verified.

This study focuses on the influence of notch prefabrication methods and prefabricated notch lengths on rock K_{IC} test results. First, the straight notches are produced by wire cutting, saw blade cutting and water jet cutting on the single-edge notched bending sample. The K_{IC} test results are compared, and the best prefabrication method is selected. And then a series of three-point bending tests with different notch lengths is carried out. In addition to investigating the impact of the notch prefabrication method and the length of notch on the K_{IC} test results, this paper also combines the test system equipped microscope, acoustic emission monitoring and field emission scanning electron microscopy to study other aspects that was less concerned by predecessors including the macroscopic damage evolution, acoustic emission process and meso-fracture characteristics of rock sample surface during the test process. The results present in this article can extend knowledge of three-point bending failure process of rock, and can also provide a certain reference for choosing a suitable three-point bending notch prefabrication method and obtaining relatively accurate K_{IC} test results.

2 Test method

2.1 Test apparatus

Based on the meso-multiaxial test device for rock failure process independently developed by Northeastern University (see Fig. 1(a)), three-point bending test fixtures, measuring sensors and microscopic observation cameras are added to realize the real-time observation of rock three-point bending testing and destruction process. The test device provides a maximum axial force of 32 kN, and the force sensor has a resolution of 1 N. Displacement-controlled loading was used throughout the test with a loading rate of 0.01 mm/min. The range of sensor measuring for rock sample mid-span deflection is 2 mm, and resolution is 0.1 μm, and the accuracy is 0.8%. The crack opening displacement sensor is installed at the prefabricated notch tip of rock sample to measure the crack opening displacement evolution during loading process. The rock sample is placed on two metal rollers. The distance between the two rollers is S=80 mm. The upper roller is loaded by a force. Before loading, the rock sample position is adjusted to ensure that the tip of the prefabricated notch is aligned with the center of the upper roller, as shown in Fig.1 (b). During the loading process, the microscopic observation camera was used to observe and record the destruction process of sample (see Fig. 1(c)). In addition, the PCI-2 system of the American Physical Acoustics Corporation (PAC) was used to monitor the acoustic emission during the three-point bending test of rock sample. The probe was in full contact with the sample using couplant, and the acoustic emission threshold was set to 40 dB.

2.2 Test plan and basic properties of rock sample

Three methods of wire cutting, saw blade cutting, and waterjet cutting were selected to prefabricate notches on granite and marble samples, and three-point rock bending tests were carried out. To reduce the discrete difference between the samples taken, the same directionality was ensured during sample preparation. After the rock sample was prepared, a complete rock sample is selected to prefabricate notches to reduce the influence of discontinuities in the rock sample on test results. The prefabricated notches must be perpendicular to the bottom edge of rock sample, as shown in Fig. 2. The length of rock sample is L=100 mm, height W=50 mm, thickness B=25 mm, and the length of the prefabricated notch is a.

Three notch prefabrication methods (wire cutting, saw blade cutting and waterjet cutting) of granite were tested with 6 samples each. There are fewer complete samples of marble, and 3 pieces of each series were tested. And then the three-point bending test of granite and marble were carried out with different prefabricated notch lengths. There were 5 series of prefabricated notch lengths. The dimensionless notch lengths ($\alpha = a / W$) were respectively represented as $\alpha = 0.1$, 0.2, 0.3, 0.4, 0.5. Six samples of each prefabricated notch length were tested for granite, and three samples of marble.

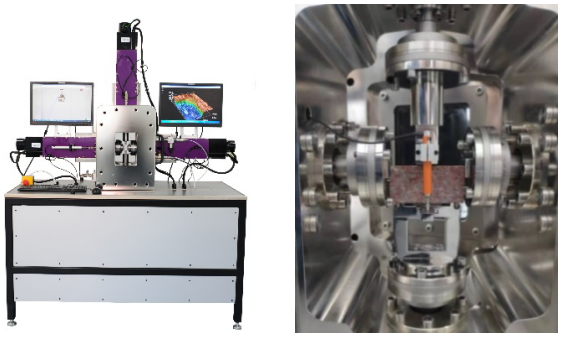

(a) Multiaxial meso-deformation apparatus (b) Interior of apparatus

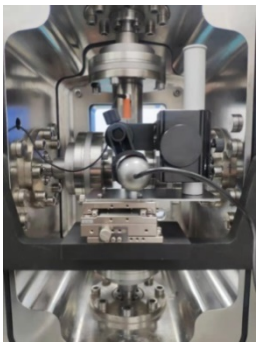

(c) Rear view of microscope system

Fig. 1 Multiaxial meso-deformation apparatus for rock fracture process

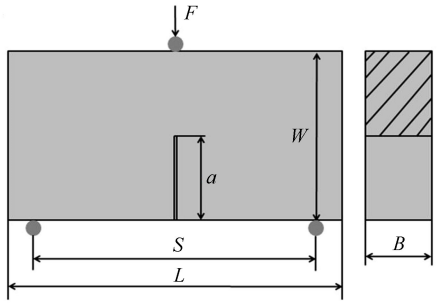

(a) Specimen size diagram

(b) Photo of specimen

Fig. 2 Size diagram and photo of specimen

The basic physical and mechanical properties of the rock samples are shown in Table 2. The mineral composition analysis of the rock sample shows that the feldspar content is about 75%, quartz content is

about 15%, and the other content is 10% in granite. The main mineral content of marble: 98% of calcite and 2% of clay minerals.

Table 2 Physico-mechanical properties of rock

Rock type	Density /(g • cm^{-3})	P-wave velocity /(m • s^{-1})	UCS /MPa	Young's modulus /GPa	Poisson's ratio
Granite	2.62	5 640	218	73.82	0.24
Marble	2.67	6 335	170	71.16	0.25

2.3 K_{IC} calculation method

During the loading process of the three-point bending test, the test system records the load and displacement of the loading point at the same time. By establishing load−displacement curves, the peak load is attained. The rock K_{IC} is calculated based on the geometrical parameters of sample, the length of the prefabricated notch, and the loading span. The K_{IC} calculation formula in this paper is given as follows [20]:

$$K_{IC} = (P_{max} S / BW^{3/2}) \cdot f(a/W) \quad (1)$$

$$f(a/W) = \frac{3(a/W)^{1/2}}{2(1+2a/W)(1-a/W)^{3/2}} \cdot \left[1.99 - (a/W)(1-a/W)\cdot(2.15 - 3.93a/W + 2.7a^2/W^2)\right] \quad (2)$$

where K_{IC} is the mode I fracture toughness of rock (MPa • m$^{0.5}$); a is the length of the prefabricated notch (mm); W is the height of the sample (mm); B is the width of the sample (mm); P_{max} is the peak load (kN) and S is the span (mm).

3 Influence of notch prefabrication methods and notch lengths

3.1 Notch prefabrication method−granite K_{IC}

Three notch prefabrication methods of wire cutting, saw blade cutting and water jet cutting were used for granite samples to conduct K_{IC} test under the condition of dimensionless notch length $\alpha = 0.5$. The test results are shown in Table 3.

Table 3 Test results of granite K_{IC} by three notch prefabrication methods

#	Wire cutting		Saw blade cutting		Water jet cutting	
	P_{max} /kN	K_{IC} /(MPa • m$^{0.5}$)	P_{max} /kN	K_{IC} /(MPa • m$^{0.5}$)	P_{max} /kN	K_{IC} /(MPa • m$^{0.5}$)
1	2.235	1.933	2.237	1.730	2.220	1.702
2	2.561	1.855	2.248	1.699	2.066	1.574
3	2.810	1.955	2.307	1.753	2.051	1.592
4	2.467	1.741	2.232	1.692	2.201	1.716
5	2.698	1.940	2.295	1.740	1.867	1.450
6	2.264	1.807	2.434	1.855	2.368	1.770
Average	2.506	1.872	2.292	1.745	2.129	1.634

It can be seen from the table that the average K_{IC} test results of wire cutting rock samples are greater than the average K_{IC} results of saw blade cutting, and the saw blade cutting value is greater than the average K_{IC} results by water jet cutting. The K_{IC} standard deviation for the wire cutting, saw blade cutting and waterjet cutting are 0.078, 0.054 and 0.107, respectively. The K_{IC} test results of granite cut by water jet have the largest dispersion, and the ones cut by saw blade make the smallest dispersion.

The samples used in this paper and those used in literature [10] are all single-edge notch bending rock samples. To compare the accuracy of calculation methods, the formula used in literature [10] are adopted for comparative calculations on the granite wire-cut series, and the results are provided in Table 4. The calculation results by the formula in this article is almost the same as the those by the formula used in literature [10], representing the formula used in this article is reliable.

Table 4 Comparison of granite K_{IC} results calculated by two different formulas

#	K_{IC} /(MPa • m$^{0.5}$)	
	Literature [10] formula results	Results from current formula
1	1.938	1.933
2	1.856	1.855
3	1.955	1.955
4	1.741	1.741
5	1.940	1.940
6	1.810	1.807
Average	1.873	1.872

Typical load−displacement curves of granite with different notch prefabrication methods are depicted in Fig. 3. Sample number G represents granite, L is the wire cutting, J is the saw blade cutting, and W is the water jet cutting. Fig.3(a) plots the curves of the three-point bending load−displacement process of granite. For the whole test process, the curve is concave at the beginning of the loading stage, and the load-to-loading point displacement curve grows nonlinearly, and then the displacement of the loading point increases linearly with increasing the load. Enlarged front section of the loading curve (as encircled by red dotted line in Fig.3(a)) are shown in Fig. 3(b). There is a significant concave section in the load−displacement curve at the beginning of the test, and then the slope of the curve gradually increases. This is due to the existence of many preexisting defects such as tiny holes and cracks in the rock. When the load increases, the preexisting defects such as holes and fissures are continuously squeezed and closed, and the rock structure tends to be compact and stable. The difference in grain composition, degree of bonding and structure results in differences in the degree of depression and the rate of slope rise of the three curves. When approaching the peak value, the growth slope of the curve slows down, and the stress drops after the peak

value. This can be observed from the monitoring of the whole test process by the platform equipped microscope. At this time, the rapid development of macro cracks caused the sample to quickly fracture into two parts, and the displacement of the loading point suddenly increased, corresponding to the curve after the peak in Fig. 3(a) developing towards the lower right.

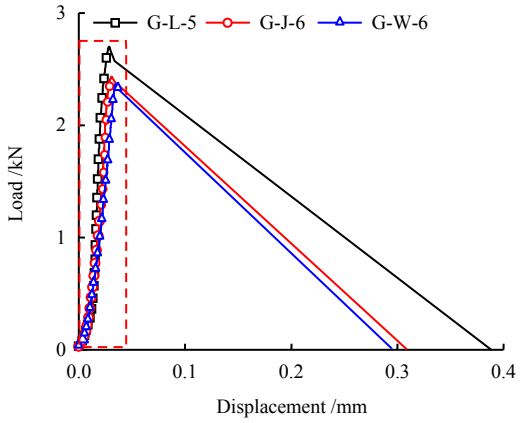

(a) Typical complete load-displacement curves

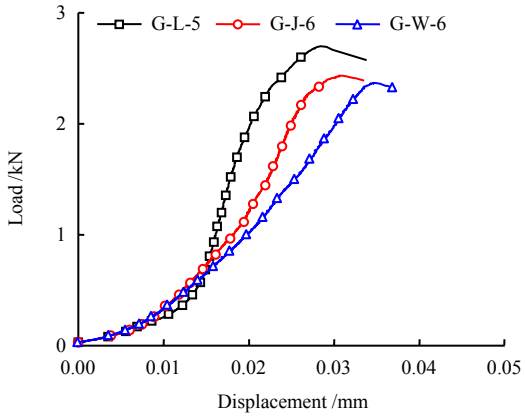

(b) Typical pre-peak load-displacement curves

Fig. 3 Load−displacement curves of typical specimens

3.2 Notch prefabrication method−marble K_{IC}

To confirm the consistency of the conclusions in section 3.1, the test scheme of marble repeating granite is adopted. Table 5 gives the marble three-point bending K_{IC} test results of different notch prefabrication methods. It can be observed that the variation law for K_{IC} test results of marble samples with different prefabrication methods are consistent with that of granite by different prefabrication methods. The wire-cut marble sample has the largest K_{IC} average, and the other two test results are all smaller. The number of test rock samples is 3, which can achieve the purpose of repeated testing. At the same time, the standard deviations of the three series of K_{IC} results are calculated as: 0.078, 0.084, and 0.200. The water jet cutting method also makes the largest dispersion of test results in marble.

Table 5 Test results of marble K_{IC} by three notch prefabrication methods

#	Wire cutting		Saw blade cutting		Water jet cutting	
	P_{max} /kN	K_{IC} /(MPa • m$^{0.5}$)	P_{max} /kN	K_{IC} /(MPa • m$^{0.5}$)	P_{max} /kN	K_{IC} /(MPa • m$^{0.5}$)
1	1.583	1.200	1.395	1.062	1.673	1.268
2	1.761	1.381	1.677	1.267	1.096	0.810
3	1.645	1.238	1.511	1.146	1.637	1.187
Average	1.663	1.273	1.528	1.158	1.469	1.088

The K_{IC} test results of granite and marble samples with different notch prefabrication methods show that the test results obtained by the wire cutting method are higher, and the results of the other two methods are lower. The K_{IC} results of the granite sample tested by the wire cutting method and the water jet cutting method differs by 14.6%, and the marble sample differs by 17%. It is evident that different notch prefabrication methods affect the test results. From the perspective of rock damage caused by cutting method, it is believed that the secondary damage caused by wire cutting method onto rock sample is smaller than the other two methods, and the measured result is closer to the true value of material. It is recommended to use wire cutting method to prefabricate notches for rock sample.

3.3 Prefabricated notch length−rock K_{IC}

Based on the analysis in sections 3.1 and 3.2, the wire cutting method was selected to prefabricate samples with different notch lengths and to test. Tables 6 and 7 summarizes the results of three-point bending tests on two rock types with 5 dimensionless notch lengths. According to the table, the peak loads of two rocks gradually decrease with the increase of notch length. The average K_{IC} values of granite with five notch lengths are 1.623, 1.749, 1.989, 1.932 and 1.872 MPa • m$^{0.5}$, respectively. The average K_{IC} values of marble with five notch lengths are 1.243, 1.288, 1.501, 1.467 and 1.273 MPa • m$^{0.5}$, respectively. Fig. 4 shows the comparison of average K_{IC} values of the two rocks with five dimensionless notch lengths. It can be clearly observed that under the five dimensionless notch lengths, the K_{IC} results of two rocks first increase and then decrease. Both kinds of rocks can obtain the maximum value of K_{IC} when the dimensionless notch length α = 0.3, and the test results obtained under the other four dimensionless notch lengths are lower.

The test results of the two rocks under different dimensionless notch lengths show that the maximum value of rock K_{IC} can be obtained at α =0.3, and the reasons are analyzed. On one hand, when the prefabricated notch is very short, the inside of the sample will experience the development of micro-cracks before the critical stress factor is reached at the crack tip for crack propagation to occur, causing an increase in the effective notch length, consequently the test results obtained are lower[28]. And

when the dimensionless notch length is small, the rock sample does not necessarily crack from the tip of prefabricated notch, but it is easily crack from recessive defects such as the loading roller or other weak planes of the sample. As shown in the literature [29], when using $\alpha = 0.16$, the crack propagation of sample is easily initiated from the loading roller, causing the test to fail. On the other hand, when the prefabricated notch is longer, the ligament length (W-a) of rock sample will be shorter, accordingly the load required for rock sample to fail will be smaller. In short, it is considered that the K_{IC} test results obtained based on the SENB specimen with a straight notch is representative when the dimensionless notch length α=0.3. To obtain the K_{IC} value which represents ultimate crack propagation resistance of rock itself, this article suggests using α=0.3 for testing.

Table 6 Test results of granite K_{IC} with different dimensionless notch lengths

#	0.1		0.2		0.3		0.4		0.5	
	P_{max} /kN	K_{IC} /(MPa • m$^{0.5}$)	P_{max} /kN	K_{IC} /(MPa • m$^{0.5}$)	P_{max} /kN	K_{IC} /(MPa • m$^{0.5}$)	P_{max} /kN	K_{IC} /(MPa • m$^{0.5}$)	P_{max} /kN	K_{IC} /(MPa • m$^{0.5}$)
1	6.355	1.694	4.928	1.705	4.836	2.230	3.567	1.962	2.235	1.933
2	6.550	1.547	4.765	1.617	4.687	2.045	3.357	1.832	2.561	1.855
3	6.700	1.669	5.355	1.820	4.492	1.797	3.748	2.040	2.810	1.955
4	6.167	1.543	5.252	1.763	5.012	1.948	3.529	1.911	2.467	1.741
5	6.685	1.610	5.529	1.857	4.699	1.806	3.818	2.084	2.698	1.940
6	6.736	1.672	5.039	1.732	4.974	2.107	3.189	1.761	2.264	1.807
Average	6.532	1.623	5.145	1.749	4.783	1.989	3.535	1.932	2.506	1.872

Table 7 Test results of marble K_{IC} with different dimensionless notch lengths

#	0.1		0.2		0.3		0.4		0.5	
	P_{max} /kN	K_{IC} /(MPa • m$^{0.5}$)	P_{max} /kN	K_{IC} /(MPa • m$^{0.5}$)	P_{max} /kN	K_{IC} /(MPa • m$^{0.5}$)	P_{max} /kN	K_{IC} /(MPa • m$^{0.5}$)	P_{max} /kN	K_{IC} /(MPa • m$^{0.5}$)
1	4.530	1.145	4.084	1.383	3.145	1.490	2.090	1.348	1.583	1.200
2	5.207	1.324	3.495	1.193	2.944	1.397	2.452	1.556	1.761	1.381
3	5.105	1.261	4.069	1.411	3.360	1.617	2.381	1.496	1.645	1.238
Average	4.947	1.243	3.790	1.288	3.150	1.501	2.308	1.467	1.663	1.273

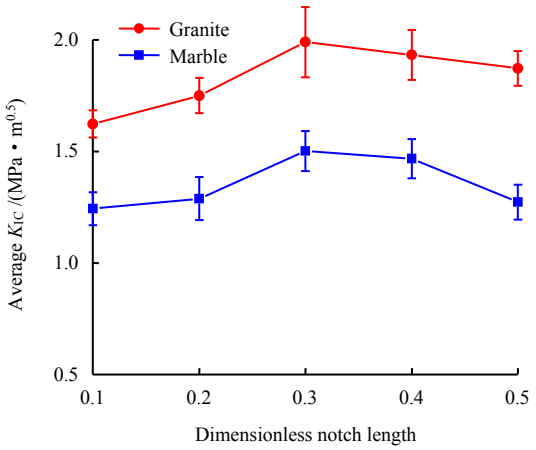

Fig. 4 Comparison of specimens K_{IC} with different dimensionless notch lengths

4 Fracture process characteristics of granite

Acoustic emission monitoring is performed on the three-point bending fracture process of granite to obtain additional details of rock sample internal fracture development. Typical rock sample G-0.4-6 is selected for acoustic emission process analysis, as shown in Fig. 5(a). There are only sporadic acoustic emission signals before the peak, and acoustic emission activities are concentrated near the peak load, which indicates that the fracture process of the rock sample has obvious brittle characteristics. According to this feature, the damage of sample is divided into three stages. Phase I (compaction and elastic phase): Acoustic emission activities are in a "quiet" phase, with very few intermittent acoustic emission signals. At this stage, the load−time curve evolves from a non-linear increase to a linear increase. Phase II (fracture evolution phase): This stage is marked by the continuous occurrence of acoustic emission activity. In Fig. 5(a), the acoustic emission signal continues to appear from point A. The internal rupture of the sample begins to develop gradually at this stage. No macro damage to the rock sample was caused. Phase III (fracture occurrence): The number of acoustic emission events peaks, and the internal fracture of the sample occurs rapidly, which finally gives rise to the macroscopic fracture of rock sample.

Figure 5(b) depicts the crack opening displacement curve and acoustic emission cumulative count curve of the rock sample. The comparison shows that the two curves have similar development trends. Both are linear in phase I, the crack opening displacement curve increases linearly, and the level of acoustic emission cumulative curve shifts linearly to the right without obvious fluctuations. The two curves in phase Ⅱ rise nonlinearly, and the slope of the corresponding crack opening displacement curve increases when the cumulative acoustic emission curve rises. When the failure occurs

in phase Ⅲ, the slope of the cumulative acoustic emission curve increases, meanwhile the crack opening displacement curve also rises rapidly with the steepest slope. Acoustic emission activity is a manifestation of the internal fracture of the sample. Literature [30] pointed out that the acoustic emission count is proportional to the internal crack growth rate of the sample. When the cumulative number of acoustic emission events in phase II in Fig. 5(b) increases, the evolution of macroscopic crack opening displacement also begins to accelerate, which implies that the crack opening displacement can be regarded as a macroscopic characterization of the specimen internal fracture. The rapid increase in the slope of crack opening displacement curve is a precursor to the failure of specimen. This result is in line with the findings from Kao et al.[31]. Kao et al. selected the number of acoustic emission events in the post-peak period and the crack opening displacement change value, and quantified the degree to which a single acoustic emission event represents an increase in the macroscopic crack opening displacement caused by micro-fracture within the sample. It means that the micro-fracture inside the sample is macroscopically manifested as an increase in the displacement of crack opening.

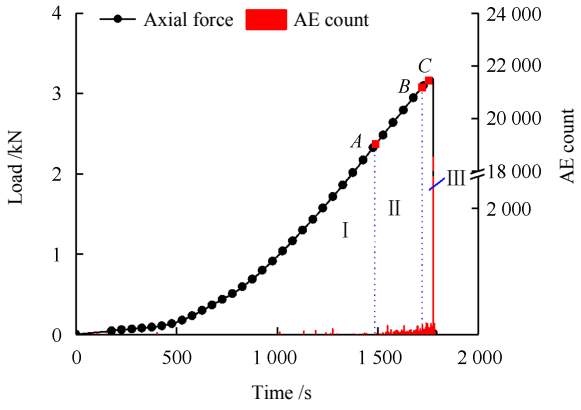

(a) Load−time curve

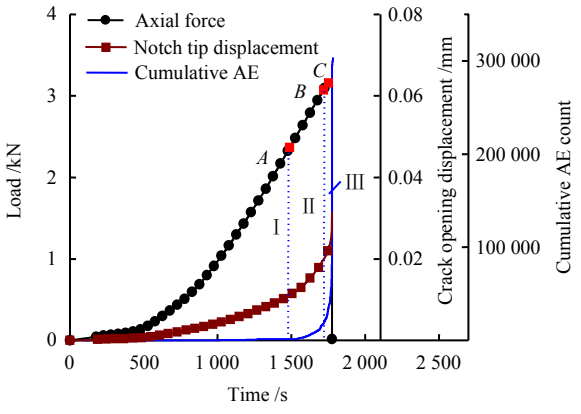

(b) Crack opening displacement and cumulative AE account curves

Fig. 5 Acoustic emission process and crack opening displacement curve of specimen G-0.4-6

The macroscopic failure development process of granite sample is recorded in real time using a rock meso-multiaxial deformation testing system equipped microscope. Figs.6(a) to 6(c) show the macroscopic failure process of sample G-0.4-6. It is found that the macroscopic failure of rock sample undergoes the evolution process of white deformation localization zone initiation, development, and final cracking failure. In Fig. 5(a), the acoustic emission signal of phase II indicates that the internal micro-cracking of sample is continuous, and a series of micro-crack propagation behaviors also occur at the tip of notch. When the test is loaded to point *B* at the end of phase II as illustrated in Fig. 5(a), micro-cracks within the sample nucleated, and linear white strips can be observed developing in the tip area of the crack on the surface of the sample with naked eye (see Fig. 6(a)). This is the macroscopic manifestation of micro-cracks inside the rock sample. This also suggests that the behavior of microscopic cracks in granite change the optical properties of rock grains to make the rock sample brighter locally and eventually develop a visible white localized zone on the surface of sample. At the same time, this white localized zone also presages the crack propagation trajectory of rock tensile failure fracture[32]. When the white deformation localization zone is fully developed and the sample is close to failure. When loaded to point *C* in Fig. 5(a), the sample is destroyed along the previously developed white deformation localization zone (see Fig. 6(b)), and finally cracks propagate up to the loading point (see Fig. 6(c)). The fracture photo of the final rock sample after failure is shown in Fig. 6(d). The crack propagation and fracture of rock sample proceed along the middle of the span, which meets the requirements of mode I fracture. The macroscopic failure evolution of the remaining granite samples observed by the equipped microscope is similar to that of sample G-0.4-6, and also undergoes the process of the white deformation localization zone initiation, development, and cracking failure.

The non-straight growth trajectory in Fig. 6(b) can be explained from the perspective of mineral grains influence of the rock sample. If the crack encounters the mineral grains during propagation process, its trajectory will be affected. Since the crack propagation tends to proceed along the direction with the least energy consumption, the cracks tend to expand along the grain boundaries. The intergranular cracks appear as tortuous crack paths in the macroscopic view and exhibits a non-linear growth pattern[33]. However, it cannot be generalized that the crack propagation path will expand along the grain boundaries when encountering the grains. Qin et al. [33] explained the propagation mode when the second phase barrier is encountered during crack

propagation process, and believes that when the stress concentration is high enough, the stress concentration will cause the crack to propagate through the obstacle.

(a) Surface deformation localization zone

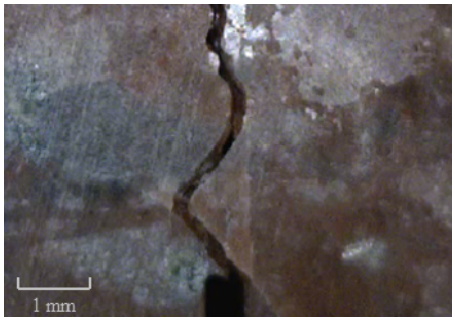

(b) Propagation along localization zone

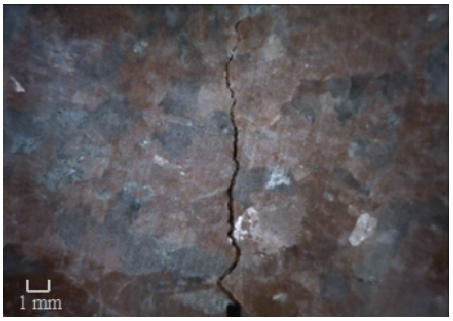

(c) Final crack propagation pattern

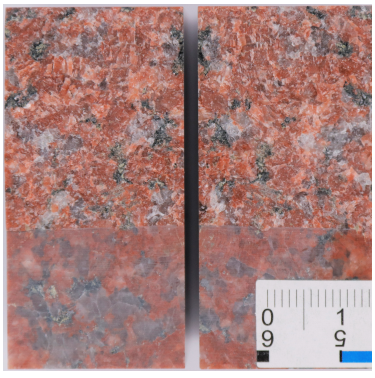

(d) Fracture of sample

Fig. 6 Macro-fracture photos of specimen G-0.4-6

5 Discussion

5.1 Influence of notch prefabrication method

The notches formed by wire cutting are uniform, without obvious undulations, protrusions or changes in notch width, and the cutting result is better. For waterjet cutting, the concentration of the water column is weakened after the high-speed waterjet penetrates the rock sample, leading to the cracks being unevenly, and some of the cracks present slightly jagged undulations. Therefore, the test results of the waterjet cutting test have the largest dispersion. The cutting quality of saw blade is better than that of waterjet cutting, but the width of the notch tip and the end of the prefabricated notch are inconsistent.

From the results of this article, although the crack width of waterjet cutting is the widest among the three prefabrication methods, the K_{IC} value obtained by the test is lower, there is a certain difference to previously obtained numerical simulation results, that is, a wider crack causes a higher peak fracture load and a larger dimensionless stress intensity factor[34−35]. This is because the numerical simulation considers the crack width as a single variable. However, in addition to the difference in the crack width, the cracks obtained by different methods in this paper also bring about varying degrees of damage, and its impact on the test results is not a single factor. This demonstrates that in the actual test, the impact of different prefabrication methods on the results should also be considered. Different cutting methods may incur new damage to the rock, which will ultimately affect the K_{IC} test results. From the perspective of notch prefabrication methods, the cutting speed of wire cutting is slow, the cracks are evenly cut, and it is unlikely to cause new damage to the rock. Although a low cutting rate is adopted in saw blade cutting and the cut notch quality is also high, the saw blade is a rigid material, thus the damage to the rock during cutting is more serious than that by wire cutting, as a result, the K_{IC} value of saw blade cutting is in the middle. The waterjet cutting speed is fast, the high-speed water flow and the garnet sand possesses a great impact on the rock sample, which triggers the initiation of new micro-cracks inside the sample. It is believed that the damage to the rock is the greatest, so its K_{IC} value is the smallest. A three-point bending K_{IC} test is carried out on rocks using different notch prefabrication methods, and the influence of different methods on the final test results is compared. This can provide a certain reference for choosing a suitable notch prefabrication method.

5.2 SEM characteristics analysis of fractures

The notch tip prefabricated by the three cutting methods represented different fracture characteristics, as shown in Fig.7. Rough undulations can be observed under the imaging of water jet cutting fracture, and the step-like cracking marks are obvious. The step-like cracking is a characteristic fracture form of the water jet cutting notch tips. The notch cut by saw blade

presents a significant river pattern. Wire cutting fractures exhibit obvious rough undulations and vertical cliffs, but the two previously mentioned characteristic patterns are rarely seen. The distribution density of river patterns is smaller than step-like patterns by waterjet cutting. The difference in SEM fracture characteristics can be attributed to the different fracture process zones within the specimen. Although it is generally considered that the fracture process zone of rock is a material constant and is related to the size of the rock mineral particles, different test conditions can lead to difference in the fracture process zone of the rock. Kuruppu et al.[36] believed that the relatively larger fracture process zone of SCB specimen is the reason for the lower K_{IC} value measured. With the help of acoustic emission, Wong et al.[37] confirmed that the fracture process zone of straight notch SCB specimen was larger than the that of Cracked Chevron Notched Semi-circular Bending specimen, and the larger the fracture process zone containing microcracks in straight notch specimen, the lower the K_{IC} is. The notches prefabricated in this paper are straight notch, but the prefabricated notches using wire-cut method can guide crack propagation more accurately than the other two prefabrication methods[15], which is similar to chevron notches. As shown in Fig. 7, the step and river pattern characteristics of waterjet cutting and saw blade cutting also characterize the development of micro-cracks at the notch tip, resulting in weak load−bearing capacity of these two series of samples, and lower K_{IC} test results. In addition, the notch tips produced by waterjet cutting and saw blade cutting are more passivated, which exposed more structural weak planes such as grain boundaries at notch tip. Under the combined action of stress concentration and rock structure weak planes, passivated notch tips are even weaker in terms of peak load bearing capacity [18].

Figure 8 displays the field emission scanning electron microscope imaging of the fracture far away of notch tip with different cutting methods. The three fracture images clearly show large cleavage fracture areas with significant brittle failure. The fractures in Fig. 8 are not as rough as the fracture tip, and there is no obvious rock debris in the imaging field. The fracture characteristics at different positions observed by SEM imaging and the stress of three-point bending test are related to the failure process. Before the stress intensity factor at the prefabricated notch tip reaches a critical value, the stress concentration effect at the notch tip becomes stronger with increasing loading. With the initiation of micro-damage in the rock, the energy is dissipated at the notch tip, causing the fracture of notch tip to be rough and make characteristic failure forms such as steps and river patterns. When the prefabricated notch begins to expand, macroscopic cracks occur rapidly, and the entire sample exhibits tensile failure. Therefore, it is believed that the fracture characteristics of notch tip are the result of energy loss during the loading process. At the far end of pre-fabricated notch, the macroscopic crack develops rapidly

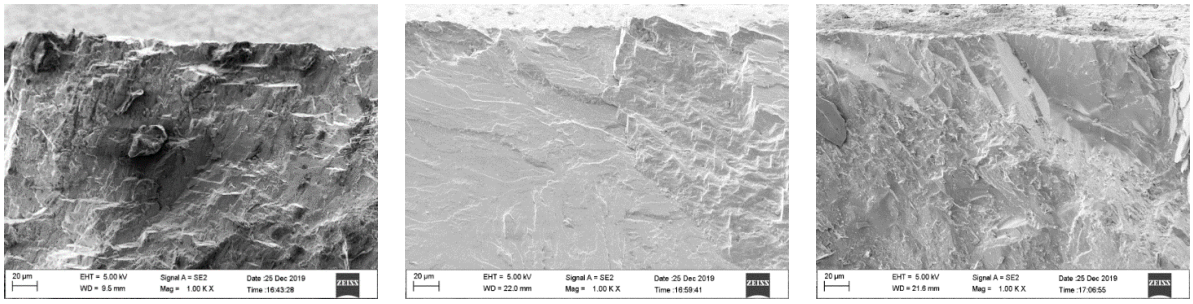

(a) Waterjet cutting (b) Saw blade cutting (c) Wire cutting

Fig. 7 SEM images of fracture surfaces near notch tips

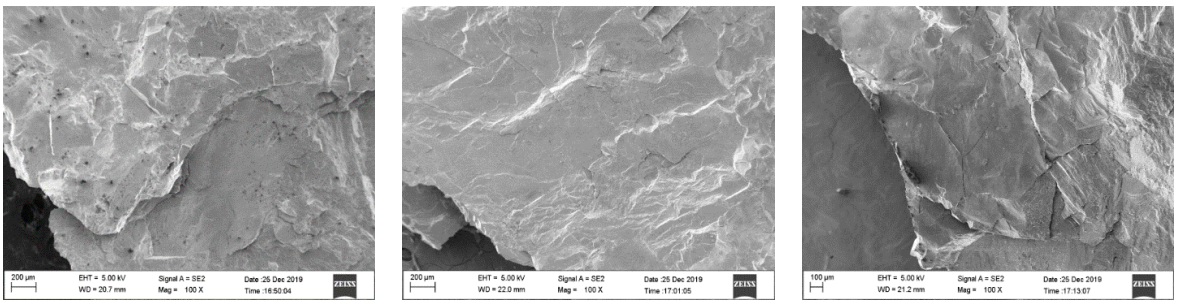

(a) Waterjet cutting (b) Saw blade cutting (c) Wire cutting

Fig. 8 SEM images of fracture surfaces away from notch tips

after the initiation of crack, and the final failure is rapid and intense. It also presents a large cleavage surface fracture with extremely obvious brittle characteristics, which is consistent with the brittle fracture characteristics reflected in the acoustic emission process.

6 Conclusion

Straight edge notch bending tests were carried out on granite and marble specimens with different prefabricated notches and different dimensionless crack lengths. The influence of notch prefabrication methods and prefabricated notch lengths on the K_{IC} test values of rock three-point bending was studied. The fractures of different prefabrication methods are compared by SEM. By combining the results from microscope camera and acoustic emission, the three-point bending macroscopic fracture failure and the internal failure evolution process of the granite sample are analyzed, and the conclusions are drawn as follows:

(1) Among the three notch prefabrication methods of wire cutting, saw blade cutting and water jet cutting, the wire cutting method has the least influence on K_{IC} test results, and the obtained K_{IC} value is higher, which is close to the true value of the material, indicating that the wire cutting method prefabrication induced damage is small.

(2) The K_{IC} of sample increases first and then decreases as the length of dimensionless prefabricated notch length increases. In this paper, the maximum value of K_{IC} can be obtained when the dimensionless crack length is $\alpha = 0.3$ out of the five kinds of cracks. It is recommended to test SENB sample with a crack length $\alpha = 0.3$ to obtain a dimensionless representative rock K_{IC} value.

(3) The macroscopic failure evolution of specimen presents a process of initiation of deformation localization zone, localization zone development, crack initiation, and final fracture failure. In the microscopic view, the fracture tip of water jet cutting sample shows a step failure characteristic, the saw blade cutting has a river-pattern-like failure characteristic, and the wire cutting rarely make the above two characteristic failure forms. The fractures far away from the notch tip exhibits large cleavage plane damage, which is not as rough as the notch tip fracture.

(4) The failure brittleness of three-point bending specimen with straight notch is obvious, and the acoustic emission events during the test are concentrated in the vicinity of load peak. The crack opening displacement curve and acoustic emission cumulative curve have a similar evolution trend. The short-term sharp increase of the sample crack opening displacement curve can be regarded as the precursor feature of the macroscopic rock sample fracture.

References

[1] GRIFFITH A A. The phenomena of rupture and flow in solids[J]. Philosophy Transaction of the Royal Society of London, 1921, 221: 163−198.

[2] IRWIN G R. Fracture dynamics[M]//Fracturing of metals. Cleveland: American Society for Metals, 1948.

[3] JI Xing. A critical review on criteria of fracture mechanics[J]. Chinese Journal of Theoretical and Applied Mechanics, 2016, 48(4): 741−753.

[4] IRWIN G R. Analysis of stresses and strains near the end of a crack tranversing a plate[J]. Journal of Applied Mechanics, 1957, 24: 361−364.

[5] ASTM. ASTM E399-70T Tentative method of test for plane strain fracture toughness of metallic materials[S]. [S. l.]: [s. n.], 1970.

[6] ATKINSON B K, YIN Xiang-chu, XIU Ji-gang. Rock fracture mechanics[M]. Beijing: Earthquake Press, 1992.

[7] CUI Zhen-dong, LIU Da-an, AN Guang-ming, et al. Research progress in mode-I fracture toughness testing methods for rocks[J]. Journal of Test and Measurement Technology, 2009, 23(3): 189−196.

[8] ISRM Testing Commission. Suggested methods for determining the fracture toughness of rock[J]. International Journal of Rock Mechanics and Mining Sciences & Geomechnics Abstracts, 1988, 25(2): 71−96.

[9] AYATOLLAHI M R, AKBARDOOST J. Size and geometry effects on rock fracture toughness: mode I fracture[J]. Rock Mechanics and Rock Engineering, 2014, 47(2): 677−687.

[10] ZUO Jian-ping, ZHOU Hong-wei, FAN Xiong, et al. Research on fracture behavior of Beishan granite after heat treatmnet under three-point bending[J]. Chinese Journal of Rock Mechanics and Engineering, 2013, 32(12): 2422−2430.

[11] MINAMI KATAOKA, EQLIMA MAHDAVI, TAKAHIRO FUNATSU, et al. Estimation of mode I fracture toughness of rock by semi-circular bend test under confining pressure condition[J]. Procedia Engineering, 2017, 191: 886−893.

[12] WU Shun-chuan, SUN Wei, LIU Yang, et al. Study on simulation method of mode I fracture toughness and its meso-influencing factors[J]. Rock and Soil Mechanics, 2020, 41(8): 2536−2546.

[13] DENG Chao-fu, LIU Jian-feng, CHEN Liang, et al. Fracture mechanical behaviors and acoustic emission characteristics of Beishan granites with different particle sizes[J]. Rock and Soil Mechanics, 2016, 37(8): 2313−2320.

[14] MINAMI KATAOKAA, SHINGO YOSHIOKAA, SANG HO CHOB, et al. Estimation of fracture toughness of

sandstone by three testing methods[C]//Proceedings of VietRock 2015 International Symposium. Hanoi, Vietnam: [s. n.], 2015.

[15] ZHAO Zi-jiang, LIU Da-an, CUI Zhen-dong, et al. Experimental study of determining fracture toughness K_{IC} of shale by semi-disk three-point bending[J]. Rock and Soil Mechanics, 2018, 39(Suppl.1): 258−266.

[16] CUI Zhen-dong, LIU Da-an, AN Guang-ming, et al. Research for determining mode I rock fracture toughness K_{IC} using cracked chevron notched Brazilian disc specimen[J]. Rock and Soil Mechanics, 2010, 31(9): 2743−2748.

[17] HUANG Jian-an, WANG Si-jing. Experimental study of the fracture toughness of rocks[J]. Chinese Journal of Geotechnical Engineering, 1982, 4(2): 67−75.

[18] ZHENG Yu-tian, ZHANG Xing, SHI Hai-yu. Experimental research on fracture toughness of rock[J]. Journal of Hydraulic Engineering, 1984(9): 19−28.

[19] TIAN Ao-shuang, WANG Xue-zhi. Effect of incision shapes of prefabricated crack on fracture toughness of concrete wedg e splitting specimens[J]. Concrete, 2011(2): 4−6.

[20] ASTM. ASTM D5045-14 Standard test methods for plane-strain fracture toughness and strain energy release rate of plastic materials[S]. [S. l.]: [s. n.], 2007.

[21] FOWELL R J. Suggested method for determining mode I fracture toughness using cracked chevron notched Brazilian disc (CCNBD) specimens[J]. International Journal of Rock Mechanics and Mining Sciences & Geomechanics Abstracts, 1995, 32: 57−64.

[22] KURUPPU M D, OBARA Y, AYATOLLAHI M R, et al. ISRM-suggested method for determining the mode I static fracture toughness using semi-circular bend specimen[J]. Rock Mechanics and Rock Engineering, 2014, 47(1): 267−274.

[23] KURUPPU M D. Fracture toughness measurement using chevron notched semi-circular bend specimen[J]. International Journal of Fracture, 1997, 86(4): 33−38.

[24] TUTLUOGLU LEVENT, KELES CIGDEM. Mode I fracture toughness determination with straight notched disk bending method[J]. International Journal of Rock Mechanics and Mining Sciences, 2011, 48(8): 1248−1261.

[25] ALIHA MRM, HOSSEINPOUR GH R, AYATOLLAHI MR. Application of cracked triangular specimen subjected to three-point bending for investigating fracture behavior of rock materials[J]. Rock Mechanics and Rock Engineering, 2013, 46(5): 1023−1034.

[26] ZHANG Sheng, WANG Long-fei, CHANG Xu, et al. Experimental study of the size effect of rock fracture toughness of limestone using the notched semi-circular bend samples[J]. Rock and Soil Mechanics, 2019, 40(5): 1740−1749.

[27] WANG Yu-suo, HU Xiao-zhi. Determination of tensile strength and fracture toughness of granite using notched three-point-bend samples[J]. Rock Mechanics and Rock Engineering, 2017, 50(1): 1−12.

[28] SUN Z, OUCHTERLONY F. Fracture toughness of stripa granite cores[J]. International Journal of Rock Mechanics and Mining Sciences & Geomechanics Abstracts, 1986, 23(6): 399−409.

[29] ZHAO Yi-xin, SUN Zhuang, LIU Bin.Comparative study of semi-circular bending tests for modes I and II fracture characteristics of Xinzhouyao bituminous coal[J]. Chinese Journal of Rock Mechanics and Engineering, 2019, 38(8): 1593−1604.

[30] ZHANG Hao, FU Dong-hui, SONG Hai-peng, et al. Damage and fracture investigation of three-point bending notched sandstone beams by DIC and AE techniques[J]. Rock Mechanics and Rock Engineering, 2015, 48(3): 1297−1303.

[31] KAO C S, CARVALHO F C S, LABUZ J F. Micromechanisms of fracture from acoustic emission[J]. International Journal of Rock Mechanics and Mining Sciences, 2011, 48(4): 666−673.

[32] ZHOU Xiao-ping, ZHANG Jian-zhi, QIAN Qi-hu, et al. Experimental investigation of progressive cracking processes in granite under uniaxial loading using digital imaging and AE techniques[J]. Journal of Structural Geology, 2019, 126(SEP.): 129−145.

[33] QIN Si-qing, LI Zao-ding, LIN Yun-mei. Research of rock fracture micro mechanism[C]//Proceedings of the Second National Conference on Rock Dynamics. Wuhan: Wuhan Technical University of Surveying and Mapping Press, 1990.

[34] DAI Feng, WANG Qi-zhi. Effects of finite notch width on stress intensity factor for CCNBD specimen[J]. Rock and Soil Mechanics, 2004, 25(3): 427−431.

[35] ZHANG Guang-qing, CHEN Mian, YANG Xiao-yuan. Influence of fracture width on rock toughness measurement[J]. Journal of China University of Petroleum (Edition of Natural Science), 2002, 26(6): 42−45.

[36] KURUPPU MAHINDA D, CHONG KEN P. Fracture toughness testing of brittle materials using semi-circular bend (SCB) specimen[J]. Engineering Fracture Mechanics, 2012, 91: 133−150.

[37] WONG LOUIS NGAI YUEN, GUO TIAN YANG. Microcracking behavior of two semi-circular bend specimens in mode I fracture toughness test of granite[J]. Engineering Fracture Mechanics, 2019, 221: 106565.